ISSN 1648-7788 / eISSN 1822-4180

VILNIUS TECH
Vilnius Gediminas Technical University

AVIATION

2024
Volume 28
Issue 4
Pages 247–254
https://doi.org/10.3846/aviation.2024.22702

DESIGN STUDY OF A MARTIAN ROTOR BLADE USING A TRIANGULAR AIRFOIL

Ndouba Ange BENAI-DARA, ZhaoLin CHEN ✉, Boureima OUEDRAOGO, Cinthia Cielo GUTIERREZ QUINO, Basil Nzubechi AGUWA

College of Aerospace Engineering, Nanjing University of Aeronautics and Astronautics, Nanjing, China

Article History:
- received 3 June 2024
- accepted 22 October 2024

Abstract. The Martian atmosphere is characterized by a low density and low speed of sound, which result in the low Reynolds number compressible flows. In this regime, conventional airfoils perform poorly due to the boundary layer separation and the formation of shack wave. The current paper investigates the hovering performance and the structure analysis of a Martian rotor blade built with a triangular airfoil using numerical analysis. The airfoil, with a thickness-chord ratio of t / c = 5% at 30% chord, has been shown through experiments to exhibit non-linear lift enhancement due to the roll-up vortex caused by the sharp leading edge at high angles of attack. The designed blade has a pitch axis of 40% chord, close to the airfoil center of gravity. In order to evaluate the blade thickness distribution along the radial station, Carbon Fiber, due to its high strength-to-weight ratio is applied to the blade. It is found that the main source of stress is inertia force rather than aerodynamic loads and that the blade is structurally safe. Finally, the blade reaches a Figure of Merit of FM = 0.73 at the collective pitch angle of 8 deg and the minimum tensile and compressive factor of safety of 2.90 and 1.74 respectively.

Keywords: numerical analysis, triangular airfoil, rotor blade design, Martian atmospheric conditions, Figure of Merit, structural analysis.

✉Corresponding author. E-mail: *zhaolin_chen@nuaa.edu.cn*

1. Introduction

The exploration of Mars planet began in 1960 and the means used to accomplish this feat were rovers, landers, and satellites which enabled to know the atmospheric conditions and the ground surface (Balaram et al., 2019). The Martian surface is steep and dominated by the massive presence of rocks and can by no means be explored effectively using these means. Therefore, NASA in collaboration with Jet Propulsion Laboratory JPL undertook the design of a helicopter to continue the exploration. Due to the significant time delay between Earth and Mars, the vehicle must be autonomous to perform the planned flight. In 2020, Mars Helicopter MH Ingenuity was successfully launched to Mars shrouded into the rover Perseverance. Ingenuity became the first autonomous Unmanned Aerial Vehicle to fly on another planet, lifting off on April 19, 2021. The vehicle weighs 1.8 kg and depends on its 1.2 m diameter two-blades counter-rotating rotors to generate thrust (Balaram et al., 2018; Grip et al., 2017; Pipenberg et al., 2019). Moreover, the rotors are designed to operate up to 2800 RPM. Large section of the blade span, $r / R \geq 0.45$ was designed using an optimized airfoil CLF 5605 and to reduce the root stress, an airfoil with higher thickness was employed (Koning et al., 2024). As for the performance, Ingenuity rotors reach a maximum Figure of Merit of $FM \approx 0.62$ with a tip Mach number of $M_{tip} \approx 0.76$ (Grip et al., 2017). In the beginning of 2024, Ingenuity performed a total of 72 flight missions including hovering and covering a distance of 17 km. Due to the incident that happened after its 72nd flight, one of the blades was damaged at the tip section bringing an end to the vehicle operation (Strickland, 2024). Recently, many researchers have explored the possibility of improving rotor performance by suggesting optimized airfoils as substitute for CLF5605 for the next generation of Mars Helicopter.

The Martian atmosphere is characterized by low density and low temperature as shown in Table 1. Unlike Earth atmospheric composition, Martian atmosphere is a Carbon dioxide-based atmosphere with 95% of CO_2, 2.7% of Nitrogen and 1.6% of Argon (Young, 2000). This atmospheric composition and the low surface temperature result in low speed of sound causing the tip Mach number to be within high subsonic range where the compressibility effect is significant. Moreover, the low density and the small rotor radius cause the chord-based Reynolds number to be less than 10^5. These two phenomena result in a regime known as the low Reynolds number compressibility regime. This regime is known to result in boundary layer separation due to the viscous effect and in the wake vortex due to the compressibility effect which both reduce the airfoil

Table 1. Martian operating conditions as used in CFD solver

Variable	Earth	Mars
Temperature, T (K)	288.15	210
Gas constant, R (m^2K/s^2)	287	199.08
Specific Heat Ratio, γ (~)	1.4	1.3
Density, ρ (kg/m^3)	1.225	0.0179
Dynamic Viscosity, μ (Ns/m^2)	$1.789x10^{-5}$	$1.13x10^{-5}$
Gravitational acceleration, g (m/s^2)	9.81	3.72
Static Pressure, p (Pa)	101300	720

performance (Chen et al., 2023; Dickinson & Gotz, 1993; Suwa et al., 2012). Koning et al. (2018), Koning (2019) and Koning et al. (2019) conducted studies on airfoils to be used in the Martian working conditions and found that the thick and cambered airfoils and sharp leading-edge airfoils with flat surfaces exhibit high lift and lift-to-drag ratio. Munday et al. (2015) conducted experimental analysis on a triangular airfoil (see Figure 1) by considering the cases of low Reynolds number incompressible flow and low Reynolds number compressible flow, typically at blade root and mean sections. The airfoil has a thickness to chord ratio of 5% at 30% chord. Both cases show linear trend at low angles of attack and non-linear lift at high angles of attack. Furthermore, a numerical analysis was conducted to unveil the source of the sudden increase in lift (Caros et al., 2022; Munday et al., 2015). And it was found that at low angles of attack, flow separation occurs at the airfoil apex creating small vortices downstream. However, as the angles of attack increase to high values, the location of the flow separation shifts to the sharp leading edge resulting in large scale vortices over the upper surface of the airfoil. As the angle of attack increases further so is the magnitude of the vortices. Based on such performance, this airfoil is selected to design the blade in order to evaluate the hover performance.

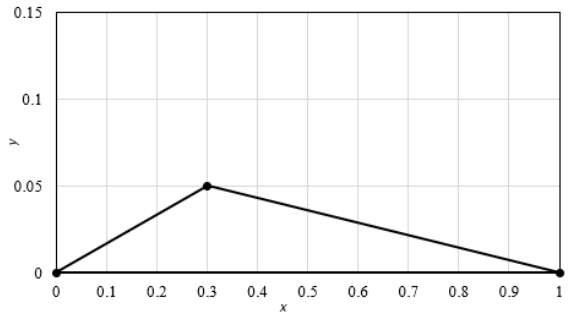

Figure 1. Triangular airfoil profile

The triangular airfoil has a maximum thickness to chord ratio of 5% at 30% chord. Due to the sharp edges of the leading and trailing edges of the airfoil, it is crucial to evaluate the thickness distribution in order to ensure the structural safety of the blade. Lumba et al. (2023) studied the effect of the pitch axis by considering 25%, 30%, 40% and 50% chord on the structural metrics of an unconventional Martian blade. The pitch axis of 40% chord is found advantageous as it keeps a good aerodynamics profile and factor of Safety. Therefore, the current pitch axis is chosen as 40% chord. The blade planform with twist distribution and the cross-section chord length along the radial station is shown in Figure 2. As the blade is in rotational motion, the tip section experiences high velocity compared to the root section (Conlisk, 2001). To compensate for the low velocity and generate linear lift distribution over the blade, the root section has to be set at a high twist angle. The twist angle of the tip section needs to be low to avoid separation or major separation. Thus, the root and tip airfoil of the designed blade have twist angles of 7 deg and 2 deg respectively.

The design of the rotor blade is a complex task involving various fields such as aerodynamics and structural analysis. However, with the advent of super computers, Computational Fluid Dynamics CFD and Finite Element Analysis FEA offer possibilities to accurately predict the performance and to perform structural analysis provided the solver has adequate resolution and appropriate grid type is used. Marinus et al. (2020) and Mian et al. (2021) compared the blade aerodynamic results obtained by low-fidelity and CFD and found that CFD results agreed well with the experimental data. Brocklehurst and Barakos (2013) employed the high-resolution CFD to gain deeper insight into blade aerodynamics and tip design. Among the adequate resolution CFD solver needs to have, is the

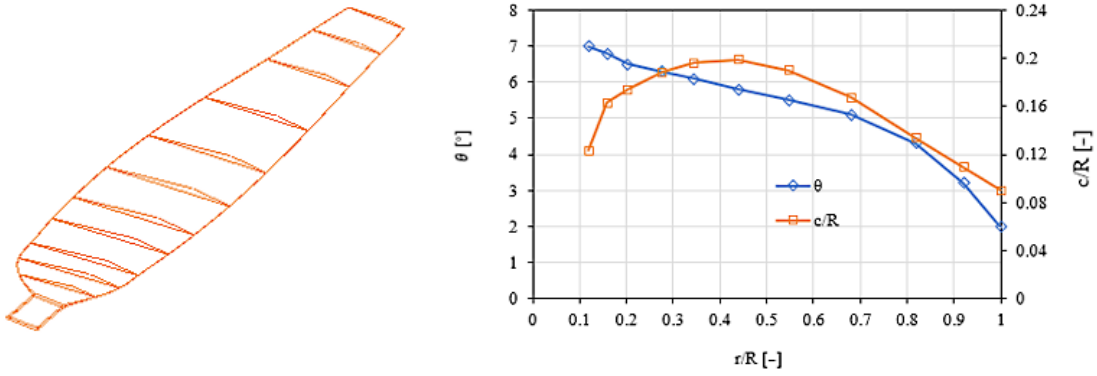

Figure 2. Blade planform with twist angle distribution and chord length along the spanwise

selection of a model. The most reliable models such as Direct Numerical Simulation DNS and Large Eddy Simulation LES are costly, especially when computing for blade aerodynamics that requires over millions of elements. An alternative to these models is Reynolds-Averaged Navier-Stokes RANS models, in particular $k-\omega$ model which have been used successfully to predict the aerodynamics characteristics of complex configurations such as high altitude-long endurance and low Reynolds number UAV propellers (Mourousias et al., 2021; Yang et al., 2023). CFD result can be coupled with the Finite Element Method to account for the blade deformations and 3D stresses resulting in Fluid-Structure Interaction FSI. Lumba et al. (2023) utilized structured grids to investigate the effects of pitch axis on the structural metrics of an unconventional Martian blade.

The current study employed numerical analysis (Fluent Solver and Static Structure) to evaluate the hovering performance and factor of safety of the blade. $k-\omega$ model associated with Shear Stress Transport SST is used as turbulence model and the pitch axis of the blade is at 40% chord. To ensure comparison with existing Martian propeller and rotor, the blade radius is similar to that of Ingenuity, R = 0.6 m (Grip et al., 2017) and the projected area similar to that designed by Lumba et al. (2023). The designed blade operates at 2800 rpm. And Carbon Fiber is used as material when conducting structural analysis (Mirdehghan, 2021).

2. Methodology

2.1. Governing equation and turbulence model

Navier-Stokes equations coupled with energy equation described the current flow pattern in the finite control volume. Fluent solver (ANSYS, 2022) is employed to evaluate the aerodynamic characteristics. The solver is based on the integral form of the governing equations where the conservation laws are enforced and large nondifferential jump is avoided. Ignoring the effect of body forces, the continuity, momentum, and energy equations are respectively given as:

$$\frac{\partial}{\partial t}\iiint_{\upsilon}\rho\, d\upsilon+\iint_{S}\rho V\cdot dS=0; \tag{1}$$

$$\frac{\partial}{\partial t}\iiint_{\upsilon}\rho V\, d\upsilon+\iint_{S}\left(\rho V\cdot dS\right)V=-\iint_{S}p\, ds+F_{viscous}; \tag{2}$$

$$\frac{\partial}{\partial t}\iiint_{\upsilon}\rho\left(e+\frac{V^2}{2}\right)d\upsilon+\iint_{S}\rho\left(e+\frac{V^2}{2}\right)V\cdot dS=\iiint_{\upsilon}\dot{q}\rho d\upsilon-\iint_{S}pV\cdot dS+\dot{Q}_{viscous}+\dot{W}_{viscous}, \tag{3}$$

where ρ is the fluid density, V and p are the freestream velocity and the pressure respectively, e and $\dot{q}$ are internal energy and volumetric rate of heat addition per unit mass respectively, $F_{viscous}$ is the viscous force, $\dot{Q}_{viscous}$ and $\dot{W}_{viscous}$ are the rate of heat and work due to viscous effects respectively. The letters υ and S denote control volume and surface.

The above equations have introduced extra unknowns resulting in much unknown parameters than equations. Assuming that the fluid is continuous since the Knudsen number $k\approx M/\sqrt{Re}<0.01$ and the molecules of the gas are calorically perfect (Hoerner, 1965), the relation between the pressure and density and temperature is given by the equation of state and that of the energy and temperature by the internal energy equation:

$$p=\rho RT \text{ and } e=C_{\upsilon}T, \tag{4}$$

where T is the temperature, R and C_{υ} are the gas constant and heat specific at constant volume respectively.

The improved version of the original $k-\omega$ model of Wilcox (Wilcox, 1988) by Menter (1994) was utilized as turbulence model. The model was combined with the Shear Stress Transport SST to account for the eddy viscosity in the adverse pressure gradient region. The transport equations of the model are given in reference (Menter, 1994).

2.2. Grid sensitivity study

CFD results depend mainly on grid density and having a good quality of the mesh with fair number of elements can minimize computational error. Kwon et al. (2015) stated that due to the complexity of propeller's geometry, the computational domain ought to be larger, from 7 to 10 blade radius in order to accurate capture the flow features of wake vortices near the blade tip. Figure 3b shows the computational domain, a half cylinder with the radius of 10 R and height of 60 R. The blade is placed at 20 R and 40 R away from the front surface and rear surface respectively. A structured mesh is used for the entire domain and the blade. Pressure-far-field is applied to inlet and outlet boundary conditions and the rotational periodic is applied to the two surfaces divided by the axis. It is worth mentioning that the flight regime of interest is hover and the aerodynamic characteristics are given as follows:

$$C_T=\frac{T}{\rho n^2D^4},\ C_P=\frac{2\pi Q}{\rho n^2D^5} \text{ and } n=\frac{RPM}{60}, \tag{5}$$

where ρ is Carbon-dioxide density, D the diameter, T and Q are the thrust and torque respectively.

To validate the grid sensitivity on the blade aerodynamics characteristics at the rotational speed of 2800 RPM, four grids with different densities are considered (see Table 2). Grid 1 is coarse with few grid elements at the blade leading edge and Grid 2 is much less coarse with some improvements in spanwise, chordwise and leading edge. Grids 3 and 4 are generated to improve the resolution of the simulation as well as to minimize the spatial discretization errors. Second order scheme is used to improve simulation accuracy and y^+ less than 1 is maintained for all the cases (Le Pape & Beaumier, 2005). Figure 4 displays the thrust and power coefficients of the four grids. It can be noticed that as the grid density increases, the result becomes more stable. Grids 1 and 2 are inappropriate as

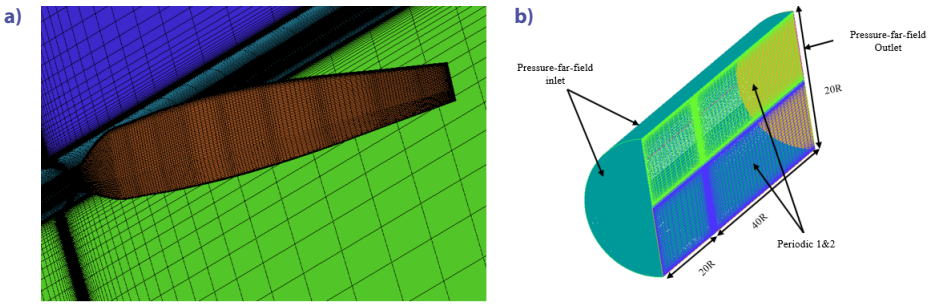

Figure 3. Grid generation: (a) – blade mesh, (b) – computational domain

the results of thrust and power coefficients are unstable. Grids 3 and 4 give a nearly stable thrust and power coefficients. Thus, taking into account the computational time and accuracy, the density for Grid 3 is adapted to the triangular airfoil blade.

Table 2. Grid independency test

Grid	No. of spanwise nodes	No. of chordwise nodes	No. of leading-edge nodes	No. of elements
Grid 1	148	45	16	3.02×10^6
Grid 2	160	50	20	3.54×10^6
Grid 3	172	55	24	4.06×10^6
Grid 4	182	60	28	4.60×10^6

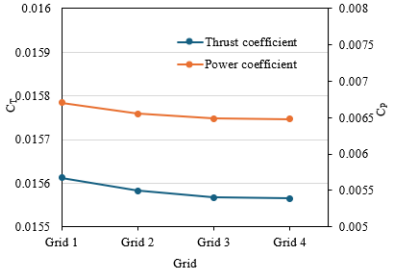

Figure 4. Comparison of Thrust and Power coefficient for the four grids

3. Results

3.1. Aerodynamics performance

The distinguished characteristics of the rotary wing vehicles are their ability to perform hovering flight regime. This flight regime is accomplished by generating thrust to offset the gravitational force. Mars gravitational acceleration is about 3.72 m/s^2 which results in the required thrust of T_{req} = 1.67 *N* for a blade considering a payload of 1.8 kg. The efficiency of a rotor at hovering is defined by the Figure of Merit given as follows (Harris, 2017):

$$FM = \sqrt{\frac{2}{\pi}}\frac{C_T^{1.5}}{C_P}, \quad (6)$$

where C_T and C_P are thrust and power coefficients respectively given in Equation (5).

Figure 5 displays the thrust and power generated by the blade over pitch angles. The designed blade with a pitch angle of 0 deg generates a thrust of T = 1.26 *N* which is below the required thrust. To ensure that the thrust requirement is met and the performance improved, the pitch angle range of [0 deg, 12 deg] with an increment of 2 is considered. The thrust force increases linearly and the power parabolically over the pitch angle range. The required thrust is attained around 1.7 deg corresponding to the power of about 37 W. As for the Figure of Merit shown in Figure 6, it increases following a non-linear trend before dropping. The pitch angle of 8 deg corresponds to the peak value of Figure of Merit *FM* = 0.73 with a thrust of T = 3.35 *N*. To examine the effect of flow separation on FM, the flow features around the blade at pitch angles of 6 deg, 8 deg and 10 deg are investigated.

The flow features i.e. Separation, Transition, Reattachment and Laminar Separation Bubble LSB are obtained through X-wall Shear plot over the cross-section airfoil of the blade. Separation point for instance is defined as the first intersection of the curve of the airfoil upper surface with x-axis. And where the curve crosses again x-axis is known as Reattachment. LSB is found as the length between

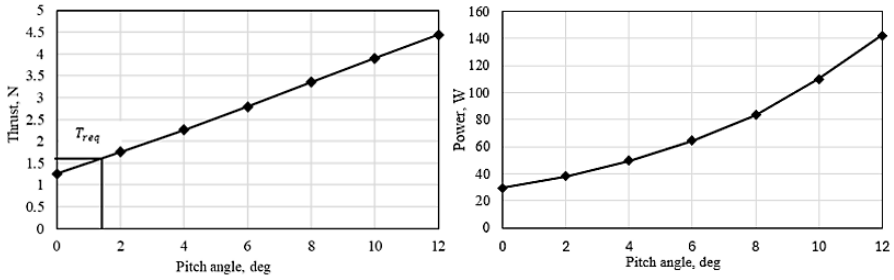

Figure 5. The thrust force and power generated by the triangular blade over the pitch angles

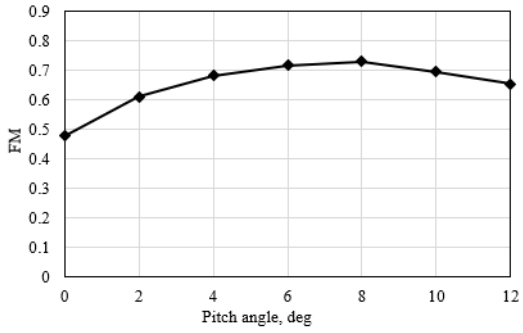

Figure 6. Figure of Merit FM over the pitch angles

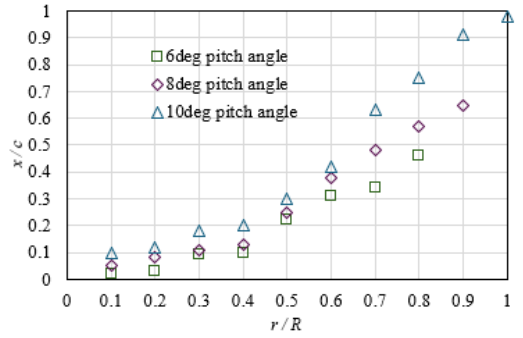

Figure 7. Separation location on the blade at pitch angles of 6 deg, 8 deg and 10 deg

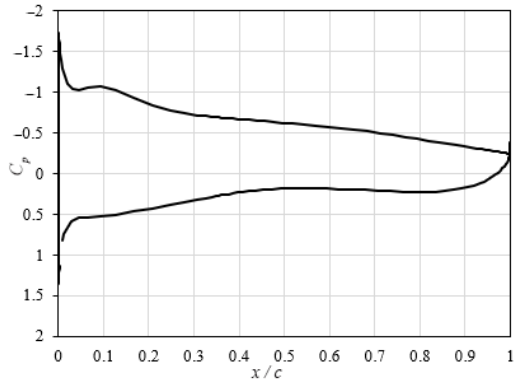

Figure 8. Pressure coefficient at r / R = 0.75

Separation and Reattachment point. Figure 7 showcases the separation location on the blade at pitch angles of 6 deg, 8 deg and 10 deg. As the blade tampers towards the tip, the separation location for all the 3 pitch angles moves away from the blade leading edge. At $r / R \leq 0.5$, the flow separates upstream the cross-section airfoil apex (x/c = 30%). However, at $r / R > 0.5$ the separation point occurs after the airfoil apex. It can be noticed that as the pitch angle increases, the more the separation point moves away from the leading edge. The blade at pitch angle of 10 deg experiences a late flow separation compared to that at 8 deg and 6 deg. Finally, the tip section of the blade at pitch angle of 6 deg and 8 deg does not experience separation. Considering the Figure of Merit and the separation location along the spanwise, the blade with the pitch angle of 8 deg is selected to examine the flow contours.

Figure 8 and Figure 9 show the pressure coefficient at r/R = 0.75 and the pressure contour around the blade at and the tip Mach number respectively. The stagnation point is observed at the blade leading edge and the pressure is unequally distributed on the blade upper and lower surfaces. Notice that the pressure on the lower surface is higher than the pressure on the upper surface which explains the thrust generation even though the flow considered in this study is compressible and the thrust is the sum of pressure force and viscous force. Yet the pressure force remains the dominant source allowing such assumption to be considered. The tip Mach number of the blade defined as the ratio of the tip velocity to the speed of sound yields a value around 0.777, less than the sonic Mach number which guarantees the transonic regime of the flow and the absence of major shock waves at pitch angle of 8 deg (Figure 9).

3.2. Structural analysis

The structural analysis known as Finite Element Method FEM of the blade was carried out using the commercial software Ansys, namely Static Structural workbench. The main purpose is to assure the structural safety of the blade under an external load. The pressure contour obtained from High-Fidelity CFD was applied on the blade surface where the blade was modeled as a shell structure, meshed in ICEM CFD and exported to Static Structural workbench.

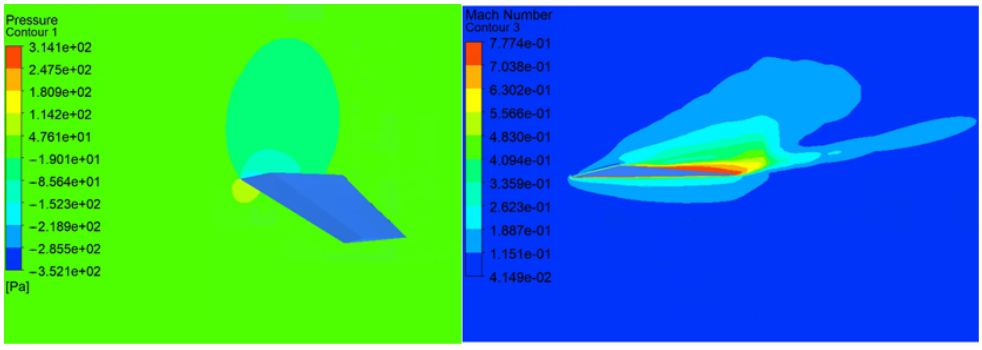

Figure 9. Pressure contour at r / R = 0.75 and tip Mach number distribution around the blade

The selection of the material was based on its compatibility with Martian atmosphere and on its weight. Table 1 displays Martian atmosphere parameters where the average temperature is roughly –60 °C. With this low temperature, materials are subject to corrosion which reduces the fatigue life. Because of its ability to resist corrosion and lightweight, Carbon Fiber was applied to the blade with its properties listed in Table 3. Figure 10 shows the structured mesh of the blade with 572054 elements along with the boundary conditions. The advantage of the structured mesh is that the matrices of the linearized equations are well structured making it simple to find an accurate solution (Chung, 1978). Moreover, the blade hub is constrained as fixed support and the blade surface is left to move. Two external loads are acting on the blade namely centrifugal force due to the rotation of the blade and aerodynamic forces (pressure contours) obtained from High-Fidelity CFD. The maximum total deformation and maximum equivalent stress are the set metrics to evaluate the structural safety of the blade.

The deformation and stress results displayed by the blade at a pitch angle of 8 deg is shown in Figure 11. The maximum deformation is at the blade tip section with the maximum value of 90.958 mm. The connection between the hub and root section experiences the stress pressure of 2086.3 MPa. The factor of safety which is defined as the ratio of Yield stress to the working stress is 2.90 and 1.74 for the minimum tensile and compressive respectively. And the maximum value of factor of safety for both components is 15 as summarized in Table 4. These results of the factors of safety are considered acceptable according to the requirement provided by NASA Technical Standard (National Aeronautics and Space Administration [NASA], 2011).

Table 3. Material properties of carbon fiber

Property	Value
Density, kg/m^3	1800
E_x, 10^{11} Pa	2.3
E_y, 10^{11} Pa	2.3
v_{xy}	0.2
G_{xy}, 10^9 Pa	9

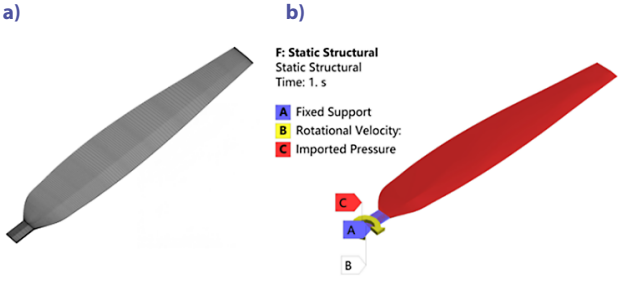

Figure 10. Blade grid and boundary conditions: (a) – structured mesh, (b) – loads applied on the blade

Table 4. Tensile and compressive factors of safety of the carbon fiber blade

Factor of safety	Minimum	Maximum
Tensile	2.90	15
Compressive	1.74	15

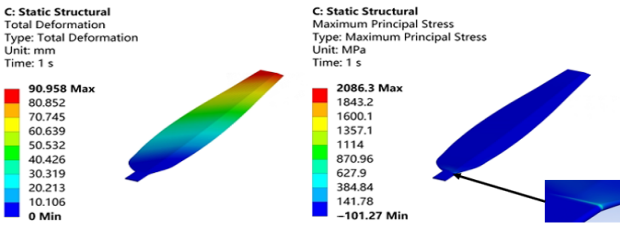

Figure 11. Deformation and stress of the blade under inertia and aerodynamics loads

4. Conclusions

The Martian atmosphere is characterized by low density and low speed of sound leading to the low Reynolds number compressible regime which reduces the performance of conventional airfoils by inducing flow separation and shock wave. The current study investigated the design study of a Martian blade built with an unconventional triangular airfoil using numerical analysis. The designed blade reached a Figure of Merit of FM = 0.73 and a thrust of T = 3.35 N at pitch angle of 8 deg with a tip Mach number of 0.777. Due to the fact that the gravitational acceleration on Mars is 3.72 m/s^2 and the required thrust per blade is 1.67 N (for a payload of 1.8 kg), the performance obtained in this study was highly beneficial to increase the ground exploration.

To ensure the thickness distribution along the radial station, the structure analysis of the blade was conducted where the pressure contour obtained from CFD solver and the inertia force were applied to the blade and Carbon Fiber was used as material. It was found that the maximum stress and deformation were 2086.3 MPa and 90.958 mm respectively and the tensile and compressive factors of safety were 2.90 and 1.74 for the minimum values respectively and 15 for the maximum values which proved the blade to be structurally safe.

Future work: Two bladed coaxial rotor configuration is known as the best configuration for Mars Helicopter. The two rotors mounted on each other can generate the required thrust over a small disk area as well as low profile drag. Moreover, the two rotors rotating in opposite directions cancel out the need for an antitorque device. Thus, future work will consider the design of the counter-rotating rotors and evaluate their performance.

Acknowledgements

I would like to sincerely thank the authors of the references used in this paper for without their publications, this paper would have no ground to stand on. A heartfelt

thanks to my supervisor Dr. Zhaolin Chen for his guidance and feedback during the redaction of this paper. I would like to extend my thankfulness to my partner Aurora along with my family, lab mates and friends for their manifold encouragement.

Funding

The author(s) disclosed receipt of the following financial support for the research, authorship, and/or publication of this article. The present work is supported by the National Natural Science Foundation of China under Grant No. 12002161, 12032011, and the National Key Laboratory of Helicopter Aeromechanics, Funding No. 2023-HA-LB-067-06.

Author contributions

NABD wrote the first draft of the paper. With the advice and guidance of ZLC, the structure and the content of the paper were improved. BO and CCGQ helped edit the content of the paper. Finally, ABN helped generate high quality figures and plots used in this paper.

Disclosure statement

Authors declare no conflict of interest.

References

ANSYS. (2022). *ANSYS-fluent solver theory guide* (*ANSYS FLUENT 2022 R1*). ANSYS.

Balaram, J. B., Canham, T., Duncan, C., Golombek, M., Grip, H. F., Johnson, W., Maki, J., Quon, A., Stern, R., & Zhu, D. (2018, January). Mars helicopter technology demonstrator. In *AIAA Atmospheric Flight Mechanics Conference* (Paper No. 2018-0023). Aerospace Research Central. https://doi.org/10.2514/6.2018-0023

Balaram, J. B., Daubar, I. J., Bapst, J., & Tzanetos, T. (2019). Helicopters on Mars: Compelling science of extreme terrains enabled by an aerial platform. In *9th International Conference on Mars 2019* (LPI Contrib. No. 2089). USRA. https://www.hou.usra.edu/meetings/ninthmars2019/pdf/6277.pdf

Brocklehurst, A., & Barakos, G. N. (2013, January). A review of helicopter rotor blade tip shapes. *Progress in Aerospace Science*, *56*, 35–74. https://doi.org/10.1016/j.paerosci.2012.06.003

Caros, L., Buxton, O., Shigeta, T., Nagata., T., Nonomura, T., Asai, K., & Vincent, P. (2022, July). Direct numerical simulation of flow over a triangular airfoil under Martian conditions. *AIAA Journal*, *60*(7). https://doi.org/10.2514/1.J061454

Chen, Z., Wei, X., Xiao, T., & Qin, N. (2023). Optimization of transonic low-Reynolds number airfoil based on genetic algorithm. *Proceedings of the Institution of Mechanical Engineers, Part G: Journal of Aerospace Engineering*, *238*(1), 1–17. https://doi.org/10.1177/09544100231207558

Chung, T. J. (1978). Finite element analysis in fluid dynamics. *Journal of Dynamics Systems, Measurement and Control, 100*(4), Article 347. https://doi.org/10.1115/1.3426389

Conlisk, A. T. (2001). Modern helicopter rotor aerodynamics. *Progress in Aerospace Sciences*, *37*(5), 419–476. https://doi.org/10.1016/S0376-0421(01)00011-2

Dickinson, M. H., & Gotz, K. G. (1993, January). Unsteady aerodynamic performance of model wings at low Reynolds numbers. *Journal of Experimental Biology*, *174*(1), 45–64. https://doi.org/10.1242/jeb.174.1.45

Grip, H. F., Johnson, W., Malpica, C., Scharf, D. P., Mandić, M., Young, L., Allan, B., Mettler, B., & Martin, M. S. (2017, September). Flight dynamics of a Mars helicopter. In *43rd European Rotorcraft Forum*, *Council of European Aerospace Societies* (*CEAS*). NASA. https://rotorcraft.arc.nasa.gov/Publications/files/ERF2017_final.pdf

Harris, F. D. (2017, December). *Hover performance of isolated proprotors and propellers – experimental data* (NASA/CR–2017–219486). Ames Research Center. https://ntrs.nasa.gov/api/citations/20180000109/downloads/20180000109.pdf

Hoerner, S. F. (1965). *Fluid-dynamic drag: Practical information on aerodynamic drag and hydrodynamic resistance.* Published by the Author.

Koning, W. J. F. (2019, July). *Airfoil selection for Mars rotor applications* (NASA/CR–019-220236). NASA. https://rotorcraft.arc.nasa.gov/Publications/files/Koning%20CR-2019-220236_FINAL.pdf

Koning, W. J. F., Johnson, W., & Grip, H. F. (2019, September). Improved Mars helicopter aerodynamic rotor model for comprehensive analyses. *AIAA Journal*, *57*(9). https://doi.org/10.2514/1.J058045

Koning, W. J. F, Perez Perez, B. N., Cummings, H. V., Romander, E. A., & Johnson, W. (2024, February). ELISA: A tool for optimization of rotor hover performance at low Reynolds number in the Mars atmosphere. *Journal of the American Helicopter Society, 69*(4), 1–15. https://doi.org/10.4050/JAHS.69.042005

Koning, W. J. F., Romander, E. A., & Johnson, W. (2018, May). Low Reynolds number airfoil evaluation for the Mars helicopter rotor. In *American Helicopter Society 74th Annual Forum* (pp. 1–17). Phoenix, AZ. https://doi.org/10.4050/F-0074-2018-12679

Kwon, H. Il., Yi, S., Choi, S., & Kim, K. (2015, Mars). Design of efficient propellers using variable-fidelity aerodynamic analysis and multilevel optimization. *Journal of Propulsion and Power*, *31*(4). https://doi.org/10.2514/1.B35097

Le Pape, A., & Beaumier, P. (2005, September). Numerical optimization of helicopter rotor aerodynamic performance in hover. *Aerospace Science and Technology*, *9*(3), 191–201. https://doi.org/10.1016/j.ast.2004.09.004

Lumba, R., Chi, C., Datta, A., Koning, W., Perez Perez, N., & Cummings, H. (2023, October). Structural design and aeromechanical analysis of unconventional blades for future Mars rotorcraft. *Journal of the American Helicopter Society*, *68*(4), 42003–42018. https://doi.org/10.4050/JAHS.68.042003

Marinus, B. G., Mourousias, N., & Malim, A. (2020, June). Exploratory optimizations of propeller blades for a high-altitude pseudo-satellite. In *AIAA Aviation 2020 Forum*. Aerospace Research Central. https://doi.org/10.2514/6.2020-2798

Menter, F. R. (1994, August). Two-equation eddy-viscosity turbulence models for engineering applications. *AIAA Journal*, *32*(8). https://doi.org/10.2514/3.12149

Mian, H. H., Wang, G., Zhou, H., & Wu X. (2021, April). Optimization of thin electric propeller using physics-based surrogate model with space mapping. *Aerospace Science and Technology*, *111*, Article 106563. https://doi.org/10.1016/j.ast.2021.106563

Mirdehghan, S. A. (2021). 1 – Fibrous polymeric composites. In *Engineered polymeric fibrous materials* (pp. 1–58). ScienceDirect. https://doi.org/10.1016/B978-0-12-824381-7.00012-3

Mourousias, N., Malim, A., Marinus, B. G., & Runacres, M. (2021, August). Surrogate-based optimization of a high-altitude propeller. In *AIAA Aviation Forum*. Aerospace Research Central. https://doi.org/10.2514/6.2021-2597

Munday, P., Taira, K., Suwa, T., Numata, D., & Asai, K. (2015). Nonlinear lift on a triangular airfoil in low-Reynolds-numbers compressible flow. *Journal of Aircraft*, *52*(3), 924–931. https://doi.org/10.2514/1.C032983

National Aeronautics and Space Administration. (2011, October). *NASA Technical Standard. Structural design and test factors of safety for spaceflight hardware*. NASA. https://standards.nasa.gov/standard/NASA/NASA-STD-5001

Pipenberg, B. T., Keennon, M. T., Tyler, J. D., Langberg, S. A., Hibbs, B., Balaram, J. B., Grip, H. F., & Pempejian, J. (2019, January). Design and fabrication of the Mars helicopter rotor, airframe, and landing gear systems. In *AIAA Scitech 2019 Forum* (Paper No. 2019-0620). Aerospace Research Central. https://doi.org/10.2514/6.2019-0620

Strickland, A. (2024, January 25). *After damaging a rotor blade, NASA's Ingenuity helicopter mission ends on Mars*. CNN. https://edition.cnn.com/2024/01/25/world/nasa-mars-ingenuity-helicopter-mission-ends-scn/index.html

Suwa, T., Nose, K., Numata, D., Nagai, H., & Asai, K. (2012, June). Compressibility effects on airfoil aerodynamics at low Reynolds number. In *30th AIAA Applied Aerodynamics Conference* (AIAA Paper 2012-3029). Aerospace Research Central. https://doi.org/10.2514/6.2012-3029

Wilcox, D. C. (1988, November). Reassessment of the scale-determining equation for advanced turbulence models. *AIAA Journal*, *26*(11). https://doi.org/10.2514/3.10041

Yang, X., Ma, D., Zhang, L., Yu, Y., Yao, Y., & Yang, M. (2023, January). High-fidelity multi-level efficiency optimization of propeller for high altitude long endurance UAV. *Aerospace Science and Technology, 133*, Article 108142. https://doi.org/10.1016/j.ast.2023.108142

Young, L. A. (2000, October). Vertical lift – not just for terrestrial flight. In *American Helicopter Society International Powered Lift Conference* (pp. 1–25). Crystal City, VA. https://rotorcraft.arc.nasa.gov/Publications/files/Young_AHS00.pdf